Eur. J. Mineral.
2013, **25**, 97–111
Published online November 2012

Shulamitite $Ca_3TiFe^{3+}AlO_8$ – a new perovskite-related mineral from Hatrurim Basin, Israel

VICTOR V. SHARYGIN[1,2,*], BILJANA LAZIC[3], THOMAS M. ARMBRUSTER[3], MIKHAIL N. MURASHKO[4], RICHARD WIRTH[5], IRINA O. GALUSKINA[6], EVGENY V. GALUSKIN[6], YEVGENY VAPNIK[7], SERGEY N. BRITVIN[8,9] and ALLA M. LOGVINOVA[1]

[1] V.S.Sobolev Institute of Geology and Mineralogy, Siberian Branch of the RAS, prosp. Akademika Koptyuga 3, Novosibirsk 630090, Russia
[2] Department of Geology and Geophysics, Novosibirsk State University, Pirogova Str. 2, Novosibirsk 630090, Russia
*Corresponding author, e-mail: sharygin@igm.nsc.ru
[3] Mineralogical Crystallography, Institute of Geological Sciences, University of Bern, Freiestrasse 3, CH-3012 Bern, Switzerland
[4] ZAO ''Systematic Mineralogy'', 11-line, 44–76, S.-Petersburg 199178, Russia
[5] Helmholtz Centre Potsdam, GFZ German Research Centre for Geosciences, Section 3.3, Telegrafenberg, 14473 Potsdam, Germany
[6] Department of Geochemistry, Mineralogy and Petrography, Faculty of Earth Sciences, University of Silesia, Będzińska 60, 41-200 Sosnowiec, Poland
[7] Department of Geological and Environmental Sciences, Ben-Gurion University of the Negev, POB 653, Beer-Sheva 84105, Israel
[8] Department of Crystallography, Faculty of Geology, St. Petersburg State University, University Emb. 7/9, St. Petersburg 199034, Russia
[9] Nanomaterials Research Center, Kola Science Center of the RAS, Fersman Str. 18, Apatity 184200, Russia

Abstract: Shulamitite, ideally $Ca_3TiFe^{3+}AlO_8$, is a mineral intermediate between perovskite $CaTiO_3$ and brownmillerite $Ca_2(Fe,Al)_2O_5$. It was discovered as a major mineral in a high-temperature larnite-mayenite rock from the Hatrurim Basin, Israel. Shulamitite is associated with larnite, F-rich mayenite, Cr-containing spinel, ye'elimite, fluorapatite, and magnesioferrite, and retrograde phases (portlandite, hematite, hillebrandite, afwillite, foshagite and katoite). The mineral forms reddish brown subhedral grains or prismatic platelets up to 200 μm and intergrowths up to 500 μm. The empirical formula of the holotype shulamitite (mean of 73 analyses) is $(Ca_{2.992}Sr_{0.007}LREE_{0.007})(Ti_{0.981}Zr_{0.014}Nb_{0.001})(Fe^{3+}_{0.947}Mg_{0.022}Cr_{0.012}Fe^{2+}_{0.012}Mn_{0.001})(Al_{0.658}Fe^{3+}_{0.288}Si_{0.054})O_8$. The X-ray diffraction powder-pattern (Mo$K\alpha$-radiation) shows the strongest lines {d [Å](I_{obs})} at: 2.677(100), 2.755(40), 1.940(40), 11.12(19), 1.585(17), 1.842(16), 1.559(16), 3.89 (13), 1.527(13). The unit-cell parameters and space group are: $a = 5.4200(6)$, $b = 11.064(1)$, $c = 5.5383(7)$ Å, $V = 332.12(1)$ Å^3, $Pmma$, $Z = 2$. The calculated density is 3.84 g/cm^3. The crystal structure of shulamitite has been refined from X-ray single-crystal data to $R1 = 0.029$ %. No partitioning among octahedral sites was found for Ti and Fe^{3+} in the structure of shulamitite, these cations are randomly distributed among all octahedra indicating an example of ''valency-imposed double site occupancy''. The strong bands in the Raman spectrum of shulamitite are at: 238, 250, 388, 561, and 742 cm^{-1}. Shulamitite from the Hatrurim Basin crystallized under combustion metamorphism conditions characterized by very high temperatures (1150–1170 °C) and low pressures (high-T-region of the spurrite-merwinite facies). Chemical data for shulamitite and its Fe-analog from other metacarbonate occurrences (natural and anthropogenic) are given here.

Key-words: shulamitite, $Ca_3TiFe_2O_8$, new mineral, perovskite, brownmillerite, crystal structure, Raman spectroscopy, Hatrurim Formation, Israel.

1. Introduction

The natural Al-rich analog of the orthorhombic synthetic phase $Ca_3TiFe^{3+}_2O_8$, an intermediate member between perovskite $CaTiO_3$ and brownmillerite $Ca_2(Fe,Al)_2O_5$, named shulamitite, was discovered in larnite rocks from the Hatrurim Basin, one of the combustion-metamorphism complexes of the Hatrurim Formation in Israel (Gross, 1977).

Synthetic Fe-rich compounds based on the perovskite and brownmillerite (perovskite-like) structure are intensively studied in material sciences due to their superconductivity

0935-1221/13/0025-2259 $ 6.75
DOI: 10.1127/0935-1221/2013/0025-2259

and ion-conductivity properties. The phase $Ca_3TiFe_2^{3+}O_8$ (Grenier phase) was firstly synthesized in the middle 1970s (Grenier *et al*., 1976, 1977). At present, three synthetic phases intermediate between perovskite $CaTiO_3$ and brownmillerite $Ca_2(Fe,Al)_2O_5$ are known to date: $Ca_4Ti_2Fe_2O_{11}$ (Gonzáles-Calbet & Valet-Regí, 1987), $Ca_3TiFe_2^{3+}O_8$ (Grenier *et al*., 1976; Rodrígues-Carvajal *et al*., 1989), and $Ca_5TiFe_2Al_2O_{13}$ (Marinho & Glasser, 1984).

Shulamitite $Ca_3TiFe^{3+}AlO_8$ was approved by the CNMNC IMA as a new mineral species in June 2011 (IMA #2011-016). The mineral name is given in honor of Dr. Shulamit Gross (1923–2012), emeritus member of the Geological Survey of Israel and famous Miss ''Mottled Zone''. The name of this reddish brown mineral is also related to biblical Shulamit, red-haired sweetheart of King Solomon. Shulamitite is major to accessory mineral in high-temperature metacarbonate larnite rocks of the Hatrurim Basin, Israel. The type sample of a larnite-mayenite rock containing abundant shulamitite (sample number M4-218, see Sharygin *et al*., 2008) is deposited in the Mineralogical Museum of St.-Petersburg State University (number 1/19465) and in the Central Siberian Geological Museum of V.S. Sobolev Institute of Geology and Mineralogy, Novosibirsk (number VII-87/1). Previously this mineral was described in the Hatrurim larnite rocks as an intermediate phase X, $Ca_3Ti(Fe,Al)_2O_8$ (Sharygin *et al*., 2008). A phase close to $Ca_3TiFe_2O_8$ was analyzed in carbonate-silicate rocks occurring as xenoliths in ignimbrites of the Upper-Chegem volcanic structure, Kabardino-Balkaria, Northern Caucasus, Russia (Galuskin *et al*., 2008, 2011). However, this natural phase (Fe-analog of shulamitite) is not yet registered as a new mineral species.

The Hatrurim Basin is a famous mineral locality (Gross, 1977; Vapnik *et al*., 2006). It is type locality for bayerite, bentorite, ye'elimite, grossite, hatrurite, nagelschmidtite (Gross & Heller, 1963; Gross, 1977, 1980, 1984; Weber & Bischoff, 1994) and barioferrite (Murashko *et al*., 2011). In this paper we provide a detailed description of shulamitite.

2. Geological background for the Hatrurim Basin

All occurrences of combustion rocks in the Hatrurim Formation (also known as ''Mottled Zone'') are located along the framing of the Jordanian-Dead Sea transform fault (Gross, 1977) and are composed of brecciated sediments (mainly carbonate-rich) and metamorphic rocks of the spurrite-merwinite facies. They occur in Israel, Jordan and Palestine. The Hatrurim Basin (approximately 5 km to southeast from Arad, latitude – 31° 12′ 45″ N, longitude – 35° 14′ 43″ E, c.a. 50 km^2, Bentor & Vroman, 1960) is the largest combustion complex of the Hatrurim Formation on the territory of Israel.

The rocks of the Hatrurim Formation in the Hatrurim Basin are the discordant cover of the Late Cretaceous carbonate, siliceous, and phosphoritic rocks of the Mishash Formation. The predominant metamorphic rocks at the Hatrurim Basin are spurrite rocks that are often localized immediately above the carbonate horizons of the section basement – the Ghareb and Mishash Formation (Gross, 1977; Burg *et al*., 1991, 1999; Sokol *et al*., 2007). Larnite rocks occur locally in the north and central parts of the complex. In the lower, middle, and upper parts of the section they form isolated bodies (up to several tens of meters long and a few meters thick) among hydrothermally altered rocks or in the direct contact with other metamorphic units. Melilite hornfelses are ubiquitous and mainly form lenses and subhorizontal sheet bodies in the section basement. Paralavas, high-temperature fused rocks, are scarce and represented by diopside–anorthite rocks ($T > 1000$ °C) in ''olive unit'' and schorlomite–pseudowollastonite–melilite species ($T > 1200$ °C) in melilite hornfels bodies (Sharygin *et al*., 2006; Vapnik *et al*., 2007; Sokol *et al*., 2008).

Most of spurrite and larnite rocks are intensely altered by low-temperature retrograde processes. They are significantly replaced by calcite, aragonite, hydrated calcium silicates and sulfates, zeolites, hydrogarnets. During these processes, identical to hydration of the Portland cement composites, fragments of combustion rocks gradually become similar to pebbles or cobbles surrounded by multilayer crusts of replacement products. Such rocks were earlier described as ''pseudo-conglomerates'' (Gross, 1977; Burg *et al*., 1991, 1999).

The ancient combustion complexes of the Hatrurim Formation, in particular the Hatrurim Basin (1–16 Ma), were earlier considered to be the products of areal combustion of bituminous chalk rocks of the Ghareb Formation (Burg *et al*., 1991, 1999 and references herein; Gur *et al*., 1995). The combustion front in subhorizontal continuous sediments was believed to reach a depth of 80–120 m. But this model contradicts with numerous geological, physical and geochemical data, because this scenario of burning is unlikely in terms of combustion physics as it rules out oxygen access to fuel particles at depth.

Most facts (in particular, the coexistence of high-temperature anhydrous rocks and low-temperature hydrothermal rocks in the Hatrurim Basin) is satisfactorily explained by the model of mud volcanism and related hydrocarbon gas combustion (Sharygin *et al*., 2006, 2008; Sokol *et al*., 2007, 2008; Vapnik *et al*., 2007). This is a process with a decrease in abnormally high pressure in beds of oil and gas provinces as a result of the ejection of gas hydrocarbons, water, and slush rock mass (mud breccia) to the surface. On repetitious explosion, gases can spontaneously ignite and burn for a long period, thus inducing combustion transformations of rocks. Later the same process was reconstructed for Nabi Musa, another locality in the Hatrurim Formation (Sokol *et al*., 2010, 2011, 2012). Combustion metamorphic rocks of the Hatrurim Basin derived from a terrigenous-carbonate protolith with different contents of clay material. The *P–T* formation conditions correspond to the spurrite-merwinite facies ($P < 25$ bars, $T = 700$–1200 °C).

Despite of different opinions on genesis, the larnite rocks of the Hatrurim Basin are considered to be the

products of the highest-temperature (900–1200 °C) solid-state reactions during combustion metamorphism (Bentor *et al*., 1963; Kolodny, 1979; Matthews & Gross, 1980; Sokol *et al*., 2005; Zateeva *et al*., 2007; Sharygin *et al*., 2008).

3. Analytical methods

The morphology and composition of shulamitite and associated minerals were investigated using JEOL JSM-35, JEOL JSM6380LA (V.S.Sobolev Institute of Geology and Mineralogy (IGM), Novosibirsk) and Philips/FEI ESEM XL30/EDAX (Faculty of Earth Sciences, University of Silesia) scanning microscopes and ''Camebax-micro'', JEOL JXA-8100 (IGM) and CAMECA SX100 (Institute of Geochemistry, Mineralogy and Petrology, University of Warsaw) electron microprobes. The composition of shulamitite was determined at an accelerating voltage of 15–20 kV, with probe current of 20–50 nA using natural and synthetic standards: wollastonite (Ca, Si), diopside (Mg), hematite (Fe), rutile and ilmenite (Ti), zircon (Zr), Cr_2O_3 (Cr), orthoclase (Al), albite (Na), $LiNbO_3$ (Nb), V_2O_5 (V), spessartine (Mn), Sr-glass (Sr), $Y_3Al_5O_{12}$ (Y), NaLa$(MoO_4)_2$ (La), LiCe$(WO_4)_2$ (Ce). Precisions for major and minor elements were better than 2 and 5 rel.%, respectively. Data reduction was performed using a PAP routine. Overlap corrections were done for the following elements: Cr$K\beta$ – Mn$K\alpha$, Si$K\alpha$ – Sr$L\alpha$.

Reflectance values for shulamitite were measured in the 400–700 nm range in air using a microscope–spectrophotometer MSFP-2 (A.A. Trofimuk Institute of Petroleum Geology and Geophysics, Novosibirsk) and a Si standard. The measured values were repeated for 16 individual grains.

Structural data of shulamitite were collected with an APEX II SMART single-crystal diffractometer (University of Bern), Mo$K\alpha$, $\lambda = 0.71073$, graphite monochromator, operated at 50 kV and 35 mA. Data were processed using the SAINT suite of software (Bruker, 2011). An empirical absorption correction using SADABS software (Sheldrick, 1996) was applied. The structure was solved by direct methods using the program SHELX97 (Sheldrick, 2008). X-ray powder diffraction data for selected shulamitite grains were obtained using a Stoe IPDS II image plate diffractometer, Gandolfi method (St. Petersburg State University). Parameters were: Mo$K\alpha$, 45 kV, 30 mA, 200 mm detector-to-sample distance, exposure 60 min. Data were processed with Stoe X-Area 1.42 and Stoe WinXPOW 2.08 program packages.

Raman spectra of single crystals of shulamitite were recorded using a Dilor XY spectrometer equipped with a 1800 line mm^{-1} grating monochromator, a charge-coupled device, Peltier-cooled detector and an Olympus BX40 confocal microscope at Bayerisches Geoinstitute, University of Bayreuth, Germany. The incident laser excitation was provided by a water-cooled argon laser source operating at 514.5 nm. The power at the exit of a 100× objective lens varied from 30 to 50 mW. Raman spectra were recorded in backscattering geometry in the range 100–4000 cm^{-1} and with a resolution of 2 cm^{-1}. Collection times of 20 s and accumulations of 5 scans were chosen. The monochromator was calibrated using the Raman scattering line of a silicon plate (520.7 cm^{-1}).

The HRTEM study of FIB-milled foils with shulamitite was performed with a TECNAI F20 X-Twin transmission electron microscope with a field emission gun FEG as electron source at Helmholtz Centre Potsdam, GFZ (Wirth, 2009). The point resolution is 0.25 nm and the lattice resolution is 0.102 nm with an information limit of 0.14 nm. The TEM is equipped with a GATAN Tridiem imaging filter GIF^{TM} and all HRTEM images were acquired as energy-filtered images applying a 10 eV window to the zero-loss peak. A careful correction of astigmatism of the objective lens was performed using the Digital Micrograph software package.

4. Sample description

Abundant shulamitite was discovered in a cobble (10 × 10 × 20 cm, M4-218, holotype sample) from ''pseudo-conglomerate'' in the central part of the Hatrurim Basin. This cobble is irregularly colored (from reddish-gray to brown) due to uneven distribution of Fe-oxide phases (spinel, shulamitite). The weathering crust is up to 5 mm and represented by hydrated Ca-silicates and ettringite. Unaltered part of the cobble is deeply dense and fine-grained. Larnite, mayenite (F-bearing species, a potentially new mineral), shulamitite, Cr-containing spinel, and sulphate-bearing fluorapatite are the major primary phases (Fig. 1, Table 1). Ye'elimite and magnesioferrite are minor and accessory minerals. The assemblage brownmillerite + unidentified K-Fe-Cu-Ni-rich sulfides + fluorapatite rarely occurs as inclusions (up 5 μm) in larnite and mayenite. Portlandite, hematite, hillebrandite, afwillite, foshagite and katoite (from $Ca_3Al_2(SiO_4)_{1.5}(OH)_6$ to $Ca_3Al_2(OH)_{12}$) represent a retrograde assemblage and are mainly confined to small vugs between grains of the primary minerals.

Shulamitite is the main Ca-ferrite of the perovskite-brownmillerite series in the holotype sample. There its abundance is up to 20 vol.%. In other larnite rocks of the Hatrurim Basin it is associated either with Fe-rich perovskite or with brownmillerite (Sharygin *et al*., 2008) and is less frequent (1–3 vol.%).

5. Morphology, optical and physical properties of shulamitite

Shulamitite from the holotype sample forms xenomorphic or subhedral grains (50–200 μm) and their intergrowths (up to 500 μm, Fig. 1). Larnite, mayenite and spinel occur as inclusions in shulamitite. Individual prismatic platelets (50–200 μm) and star-like aggregates (twins, up to 200 μm) are also common (Fig. 2). Prismatic crystals have

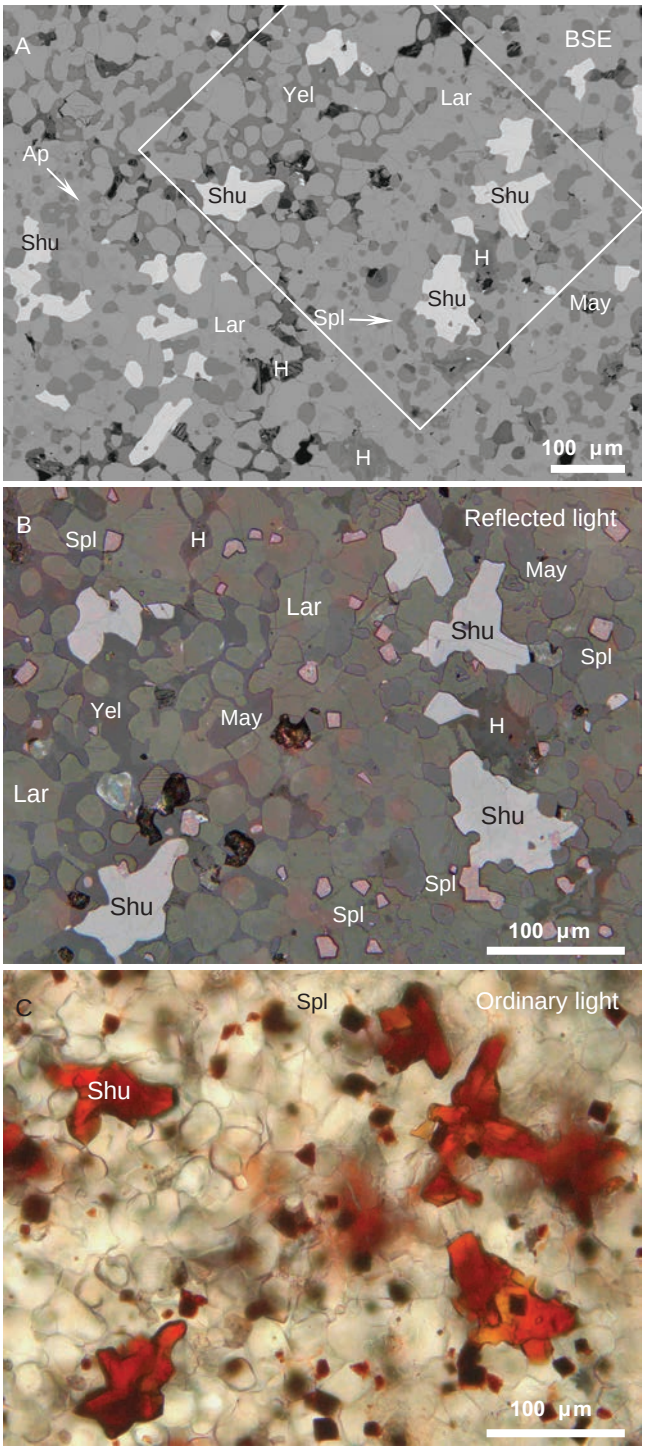

Fig. 1. General view of larnite-mayenite rock from the Hatrurim Basin containing shulamitite (holotype sample M4-218). Framed area shows shulamitite grains magnified on Figures B–C. Symbols: Shu – shulamitite, May – mayenite, Ap – fluorapatite, Yel – ye'elimite, Spl – Cr-containing spinel, Lar – larnite, H – hydrated phases in vugs.

following forms: {100}, {010} and {001}, rhombic prisms are minor. The simple (in 90°) and complex (in 90°, 45° and 60°) twinning is common for shulamitite (Fig. 2 C–F).

The color of shulamitite is reddish brown. In thin section, the color varies from reddish brown to yellow brown. Under reflected light shulamitite is gray to light gray and shows characteristic yellow brown internal reflections. Bireflectance and anisotropy are weak, pleochroism is distinct from gray to light gray. The reflectance data for the mineral are given in Table 2. The color of the powdered mineral is light brown. Shulamitite has adamantine to submetallic luster. Its hardness is 6–7 (Mohs), microhardness VHN_{100} = 683–977 kg/mm^2, mean 866 kg/mm^2. Cleavage is good on (010) and imperfect on (001) and (100), fracture is even to uneven. Density was not measured because of small grain size and common inclusions. Density in the range 3.84–3.865 g/cm^3 was calculated from unit-cell dimensions, refined or assigned scattering power at structural sites and results of electron-microprobe analyses.

Shulamitite is weakly resistant to weathering or retrograde alteration, sometimes transforming into a hydrated phase $CaTiFe^{3+}AlO_8 \cdot 2–3H_2O$ (Fig. 3). In the vugs this hydrated oxide, occasionally with shulamitite relics, is associated with other retrograde minerals (portlandite, hematite, katoite and various calcium hydrosilicates).

6. Chemical composition of shulamitite

Holotype shulamitite (sample M4-218) does not essentially vary in chemical composition (Table 3). The mineral is practically uniform within individual grains and their core-to-rim variations are negligible. Its empirical formula (means of 73 analyses) is $(Ca_{2.992}Sr_{0.007}LREE_{0.007})(Ti_{0.981}Zr_{0.014}Nb_{0.001})$ $(Fe^{3+}_{0.947}Mg_{0.022}Cr_{0.012}$ $Fe^{2+}_{0.012}Mn_{0.001})$ $(Al_{0.658}Fe^{3+}_{0.288}$ $Si_{0.054})O_8$. In general, the Ti content of holotype shulamitite is close to 1 apfu and its average formula is $Ca_3TiFe(Al_{0.7}Fe_{0.3})O_8$. The contents of minor elements are insignificant (in apfu): Si – up to 0.06; Zr, Cr and Mg – up to 0.02; Sr and REE – up to 0.01.

However, shulamitite from other larnite rocks of the Hatrurim Basin differs from the holotype in higher Al and occasionally Cr (Table 3). In addition, some compositions show the predominance of Fe^{3+} over Al^{3+} at the tetrahedral site. Nominally such compositions are related to the Fe-analog of shulamitite $Ca_3TiFe(Fe,Al)O_8$ assuming the possible existence of the solid solution $Ca_3TiFeAlO_8$-$Ca_3TiFeFeO_8$. It should be noted that shulamitite at Hatrurim Basin is common in mayenite-containing larnite rocks; whereas the Fe-analog was found only in ye'elimite-bearing larnite rocks (Sharygin *et al.*, 2008).

7. Crystal structure

The single-crystal X-ray study yielded the orthorhombic symmetry: a = 5.4200(6), b = 11.064(1), c = 5.5383(7) Å, V = 332.12(1) Å^3.The shulamitite structure was refined to R = 0.0290 in space group *Pmma* (no. 51) (Tables 4–7, Figs. 4–5). Shulamitite has a G-type structure (Grenier

Table 1. Main minerals associated with shulamitite in larnite-mayenite rock (holotype sample M4-218), Hatrurim Basin.

	Larnite	Mayenite	Spinel				Apatite	
n	7	13	1	1	1	1	1	4
			c	r	c	r		
(wt%)								
SO_3	n.d.	n.d.					7.41	4.77
P_2O_5	1.79	n.d.					28.43	32.47
V_2O_5							0.40	0.36
SiO_2	32.79	0.54	n.d.	n.d.	n.d.	n.d.	5.78	3.90
TiO_2	0.17	0.02	0.08	0.18	0.12	0.13	n.d.	n.d.
Cr_2O_3	n.d.		11.98	3.55	6.39	1.72		
Al_2O_3	0.24	45.41	40.57	45.04	46.51	47.27	n.d.	n.d.
Fe_2O_3		2.79	20.97	22.97	18.81	24.04		
FeO	0.03		4.87	7.61	5.13	4.18	0.05	0.04
MnO	n.d.	0.02	0.10	0.10	0.10	0.12	n.d.	n.d.
MgO	n.d.	n.d.	21.33	19.85	21.56	22.36	n.d.	n.d.
NiO			0.08	0.08	0.06	0.10		
ZnO			0.30	0.30	0.33	0.33		
CaO	64.17	44.68	0.39	0.50	0.37	0.49	55.11	55.48
SrO	0.22	0.12					0.49	0.36
Na_2O	0.39	0.04						
K_2O	0.28	0.02					n.d.	n.d.
F		2.77					3.67	3.76
Cl		0.08					n.d.	n.d.
H_2O*		4.60					0.04	0.01
$O=(F,Cl)_2$		1.18					1.55	1.58
Total	100.08	99.88	100.67	100.18	99.38	100.74	99.83	99.57
Calculated on								
Anions	4		4	4	4	4		
Cations		26	3	3	3	3	10 Ca	10 Ca
S^{6+}							0.936	0.600
P^{5+}	0.044						4.050	4.601
V^{5+}							0.045	0.040
Si	0.940	0.134					0.973	0.652
Ti	0.004	0.004	0.002	0.004	0.003	0.003		
Cr			0.259	0.076	0.136	0.036		
Al	0.008	13.351	1.307	1.445	1.477	1.478		
Fe^{3+}		0.524	0.431	0.471	0.381	0.480		
Fe^{2+}	0.001		0.111	0.173	0.116	0.093	0.007	0.006
Mn		0.003	0.002	0.002	0.002	0.003		
Mg			0.869	0.806	0.866	0.885		
Ni			0.002	0.002	0.001	0.002		
Zn			0.006	0.006	0.007	0.006		
Ca	1.970	11.941	0.011	0.015	0.011	0.014	9.945	9.959
Sr	0.004	0.017					0.048	0.035
Na	0.022	0.021						
K	0.010	0.005						
F		2.187					1.953	1.990
Cl		0.033						
OH		0.100					0.047	0.010
H_2O		3.780						

n – average of analyses, c, r – core and rim of grain, n.d. – not detected. * – H_2O in mayenite is calculated from ideal formula $Ca_{12}Al_{14}O_{32}\{(H_2O)_4F_2\}_6$ (Galuskin *et al*., 2012), where H_2O = 6-(F,Cl) in apfu, OH (apfu) is calculated from charge balance. H_2O in fluorapatite is calculated from formula as (OH) = 2-F (in apfu). 10 Ca – formula based on total cations in the Ca site. Fe_2O_3 and FeO in spinel are calculated from charge balance.

et al., 1976) intermediate between the perovskite (P) and brownmillerite (B) structure. In analogy to the high-T_c superconductors in the system Y–Ba–Cu–O, shulamitite has a three-fold superstructure of cubic perovskite: $\mathbf{a}_c \times \sqrt{2}$, 3 $\mathbf{a}_c$, $\mathbf{a}_c \times \sqrt{2}$. The structure of synthetic $Ca_3TiFe_2O_8$ (Rodrígues-Carvajal *et al*., 1989) has been refined from X-ray powder data in the acentric space group $Pcm2_1$ (no. 26). *Pmma* (standard setting) is the centrosymmetric counterpart of $P2_1ma$ (no. 26), which is related to the standard setting $Pcm2_1$ by interchange of **a** and **c**. The major difference between the ordered (acentric) and disordered (centrosymmetric) model is an ordered arrangement of chains formed by $Fe^{3+}O_4$ tetrahedra in the acentric structure (Fig. 4). In the disordered structure of shulamitite there

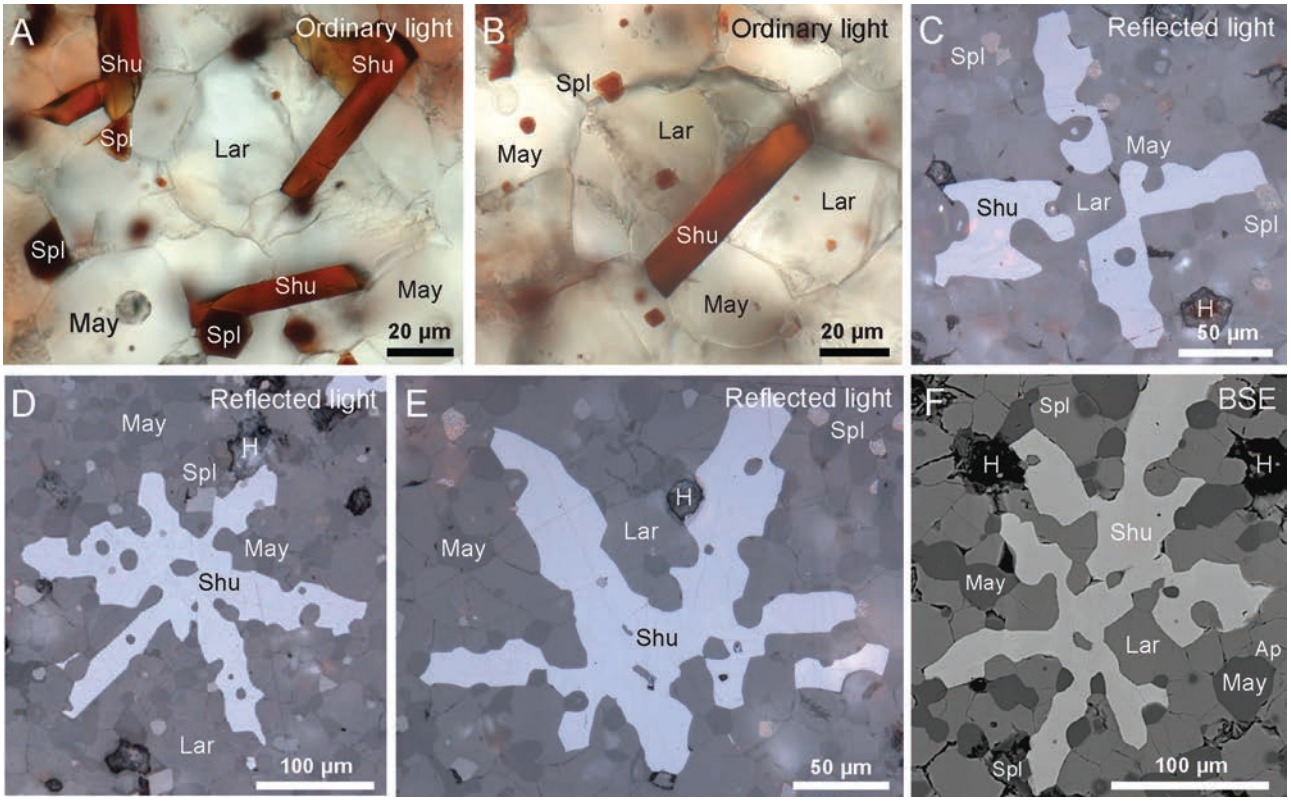

Fig. 2. Individual crystals (A–B) and star-like aggregates (C–F) of shulamitite, Hatrurim Basin (holotype sample). Symbols see Fig. 1.

Table 2. Reflectance values for shulamitite.

nm	R_{max}/R_{min}	nm	R_{max}/R_{min}
400	14.6/13.4	560	13.1/12.2
420	13.6/12.5	580	12.5/11.7
440	13.3/12.2	**589**	**12.3/11.6**
460	12.9/11.9	600	12.2/11.6
470	**12.6/11.7**	620	12.2/11.5
480	12.5/11.6	640	12.3/11.5
500	12.6/11.6	**650**	**12.3/11.4**
520	12.3/11.4	660	12.3/11.4
540	12.2/11.4	680	11.9/11.3
546	**12.4/11.6**	700	11.7/11.2

Bold – interpolated values.

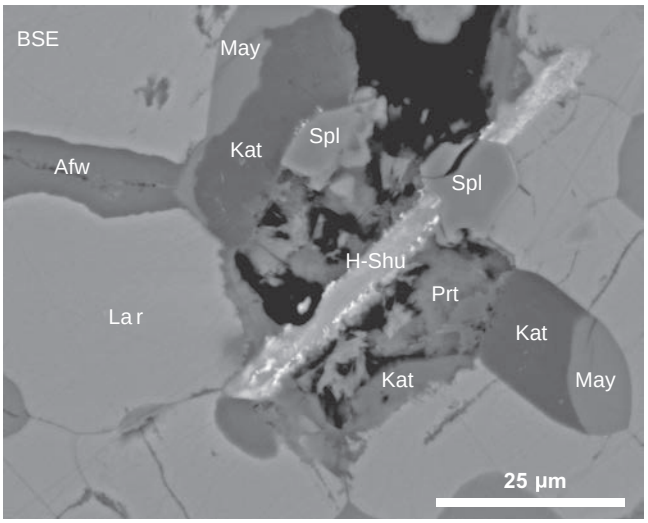

Fig. 3. In vugs shulamitite is replaced by a hydrated phase $CaTiFe^{3+}AlO_8 \cdot 2\text{-}3H_2O$ (holotype sample, Hatrurim Basin). H-Shu – replaced shulamitite, Afw – afwillite, Kat – katoite, Prt – portlandite, other symbols see Figs. 1–2.

are two randomly distributed orientations of (Al,Fe^{3+}) chains (Fig. 5). It should be mentioned that besides fully ordered ($P2_1ma$) or disordered ($Pmma$) structure a more complex ordering within the tetragonal layers is possible, for example with low or no correlation between adjacent sheets, as found in many brownmillerite compounds (Krüger *et al.*, 2011). However, our structural data do not allow distinguishing the origin of these two orientations as result of 50:50 twinning of the acentric model or as statistical disorder. As a consequence of the assumed disorder the tetrahedrally coordinated site (Fe2,Al2) and O2 are only half occupied (Table 5). In addition, the interspace (viewed along **b**) between the corner-sharing (Fe^{3+},Ti) octahedra in the ordered structure has a trapezoid cross-section whereas the corresponding cross-section in the disordered structure is almost quadratic (Fig. 4).

In general, the structural data for both shulamitite and synthetic $Ca_3TiFe_2O_8$ (Rodrígues-Carvajal *et al.*, 1989)

Table 3. Chemical composition of shulamitite and its Fe-analog from the Hatrurim Basin, Israel.

Sample	1 M4-218	s.d.	Range	2	3	4	5	6	7 M4-251	8 M5-32	9 H-201	10 M5-31
n	20			17	18	16	1	1	7	5	2	10
(wt%)												
SiO_2	0.80	0.08	0.65–0.97	0.92	0.80	0.83	0.72	0.82	0.55	0.65	0.60	1.07
TiO_2	20.39	0.23	19.93–20.76	20.19	20.29	20.13	20.03	19.86	20.41	19.91	18.59	17.85
ZrO_2	0.49	0.06	0.33–0.59	0.46	0.45	0.40	0.46	0.46	0.49	0.55	0.35	0.41
Nb_2O_5				0.04		0.04	n.d.	0.02	0.02	0.05		0.07
Cr_2O_3	0.30	0.09	0.17–0.42	0.22	0.20	0.25	0.29	0.15	0.30	3.37	0.45	0.35
Al_2O_3	8.82	0.24	7.93–9.13	8.28	8.85	8.71	8.43	8.63	9.97	9.69	4.85	5.62
Fe_2O_3	25.04	0.75	23.94–27.40	25.58	25.60	25.70	26.54	25.98	23.66	21.55	32.27	31.65
FeO	0.11	0.08	0.00–0.28	0.36	0.37	0.04		0.02	0.17			
MnO					n.d.	n.d.	n.d.	n.d.	n.d.	n.d.	0.05	0.05
MgO	0.22	0.06	0.08–0.33	0.25	0.26	0.19	0.15	0.15	0.12	0.27	0.12	0.20
CaO	43.75	0.22	43.39–44.14	42.85	42.95	43.60	43.62	43.35	43.42	43.21	42.48	42.61
SrO				0.21	0.20	0.15	0.13	0.20	0.22	0.21	0.20	0.17
Y_2O_3				0.04						n.d.		n.d.
La_2O_3				0.13					0.08	0.19		0.14
Ce_2O_3				0.15					0.11	0.19		0.18
Na_2O				0.03	0.03	n.d.	n.d.	n.d.		0.05		0.04
Total	99.92	0.39	99.20–100.78	99.71	100.00	100.04	100.37	99.64	99.52	99.89	100.03*	100.41
Formulae calculated on 6 cations and 8 oxygens												
Si	0.052			0.059	0.051	0.053	0.046	0.053	0.035	0.042	0.040	0.070
Al	0.669			0.634	0.672	0.661	0.639	0.658	0.758	0.734	0.377	0.433
Fe^{3+}	0.279			0.307	0.276	0.286	0.314	0.289	0.207	0.224	0.583	0.497
Tetrahedra	1.000			1.000	1.000	1.000	1.000	1.000	1.000	1.000	1.000	1.000
Ti	0.988			0.986	0.985	0.975	0.970	0.967	0.991	0.964	0.921	0.879
Zr	0.015			0.014	0.014	0.012	0.014	0.015	0.015	0.017	0.011	0.013
Nb				0.001		0.001		0.001	0.001	0.001		0.002
Cr	0.015			0.011	0.010	0.013	0.015	0.007	0.015	0.171	0.024	0.018
Fe^{3+}	0.934			0.942	0.966	0.960	0.971	0.977	0.941	0.819	1.016	1.060
Fe^{2+}	0.006			0.020	0.020	0.002		0.001	0.009			
Mn											0.003	0.003
Mg	0.021			0.024	0.025	0.018	0.014	0.014	0.012	0.026	0.012	0.019
Octahedra	1.979			1.998	2.020	1.981	1.984	1.982	1.984	1.998	1.991*	1.994
Ca	3.021			2.982	2.969	3.012	3.011	3.010	3.003	2.978	3.001	2.988
Sr				0.008	0.008	0.006	0.005	0.007	0.008	0.008	0.008	0.006
Y + REE				0.008					0.005	0.010		0.008
Na				0.004	0.003					0.006		0.004
Polyhedra	3.021			3.002	2.980	3.018	3.016	3.017	3.016	3.002	3.009	3.006
End-members												
$Ca_3TiFeAlO_8$	66.92			63.33	67.24	66.08	63.95	65.84	75.80	73.43	37.67	43.28
$Ca_3TiFeFeO_8$	27.91			30.72	27.62	28.58	31.42	28.86	20.68	22.39	58.36	49.69
$Ca_3Ti(Fe,Mg)SiO_8$	5.17			5.95	5.14	5.34	4.63	5.30	3.52	4.18	3.97	7.03

n – number of analyses; V_2O_3, NiO and K_2O are below detection limits ($\ll$ 0.01 wt%). Fe_2O_3 and FeO are calculated from charge balance. All alumina is considered to be in the tetrahedral site. 1–6 – holotype shulamitite: 1 – composition for the crystals used for structural research; 2–6 – compositions analyzed by different elemental suite; 5–6 – core and rim of individual crystal; 7–8 – shulamitite from other samples; 9–10 – Fe-analog of shulamitite. M4-218, M4-251, M5-32 – larnite-mayenite rocks; H-201, M5-31 – larnite-ye'elimite rocks (see Sharygin *et al*., 2008). * – totals include 0.07 wt% ZnO and 0.004 apfu Zn.

show that there is no preferred octahedral site for Ti, and the main cations Fe^{3+} and Ti are randomly distributed in all octahedra. In this sense both phases are examples of ''valency-imposed double site occupancy'' (Hatert & Burke, 2008). Site occupancy refinements for octahedral and tetrahedral sites in shulamitite indicate that the majority of Al has tetrahedral coordination and Al is the dominant tetrahedral cation. In addition, ca. 10% of the octahedra are occupied by light elements such as Al and minor Mg. Structural data for shulamitite yield the composition $Ca_3TiFe^{3+}_{0.80}(Al,Mg)_{0.20}(Al_{0.62}Fe^{3+}_{0.38})O_8$ (Table 5) very close to the result obtained by microprobe data $Ca_{3.021}Ti_{0.987}$ $Zr_{0.015}Fe^{3+}_{0.934}Mg_{0.021}Cr_{0.015}Fe^{2+}_{0.006}(Al_{0.669}Fe_{0.279}Si_{0.052})O_8$ (analysis 1, Table 3). The X-ray diffraction powder-pattern is listed in Table 8.

According to the $CaTiO_3$–$Ca_2Fe_2O_5$ phase diagram (Becerro *et al*., 1999, 2000, 2002), the phase $Ca_3TiFe_2O_8$ (Grenier *et al*., 1976; Rodrígues-Carvajal *et al*., 1989; Cherepanova & Tsybulya, 2008) should be stoichiometric without vacancies. Any deviations from Ti = 1 (apfu)

Table 4. Data collection and structure refinement details for shulamitite.

Temperature	296 (2) K
Theta range for data collection	to 31.47°
Index ranges	$-6 \leq h$ 7, $-16 \leq k \leq 15$, $-7 \leq l \leq 7$
Reflections collected	3785
Independent reflections	605 [$R_{(int)} = 0.033$]
Crystal size	0.02 × 0.04 × 0.05 mm
Crystal system	Orthorhombic
Space group	*Pmma*
Unit cell dimensions	$a = 5.4200$ (6) Å $b = 11.064$ (1) Å $c = 5.5383$ (7) Å
Volume	332.12 (1) Å^3
Z	2
Number of refined variables	52
Density (calculated)	3.84 g/cm^3
Goodness-of-fit on F^2	1.294
Final *R* indices	533 data; $I > 2\sigma(I)$, $R1 = 0.0290$ 605 all data $R1 = 0.0343$, $wR2 = 0.0644$

Table 5. Atom coordinates, $U_{eq.}$ (Å^2) and site occupancies for the average structure of shulamitite.

Site	Atom	*x*	*y*	*z*	U_{eq}	Occupancy
Ti1	Ti	0.2500	0.17018 (5)	0.23942 (11)	0.0062 (2)	0.50
Fe1	Fe					0.400 (6)
Al1	Al					0.100 (6)
Fe2	Fe	0.1998 (3)	0.5000	0.1794 (3)	0.0064 (6)	0.188 (4)
Al2	Al					0.312 (4)
Ca1	Ca	−0.2500	0.31440 (7)	0.27827 (14)	0.0126 (2)	1
Ca2	Ca	0.2500	0.0000	−0.2663 (2)	0.0139 (3)	1
O1	O	0.2500	0.3599 (3)	0.3214 (5)	0.0183 (7)	1
O2	O	0.1362 (11)	0.5000	−0.1110 (10)	0.0148 (12)	0.50
O3	O	0.0000	0.1521 (2)	0.5000	0.0118 (6)	1
O4	O	0.2500	0.0000	0.1722 (7)	0.0130 (8)	1
O5	O	0.0000	0.2023 (3)	0.0000	0.0143 (6)	1

Table 6. Anisotropic displacement parameters (Å^2) for shulamitite.

Site	U_{11}	U_{22}	U_{33}	U_{23}	U_{13}	U_{12}
Ti, Fe, Al1	0.0043 (3)	0.0086 (3)	0.0056 (3)	0.0006 (2)	0.000	0.000
Al, Fe2	0.0073 (14)	0.0041 (6)	0.0078 (6)	0.000	−0.0012 (5)	0.000
Ca1	0.0202 (4)	0.0088 (4)	0.0088 (4)	−0.0002 (3)	0.000	0.000
Ca2	0.0164 (6)	0.0119 (5)	0.0133 (5)	0.000	0.000	0.000
O1	0.0326 (19)	0.0116 (13)	0.0108 (13)	0.0017 (10)	0.000	0.000
O2	0.019 (3)	0.012 (3)	0.013 (2)	0.000	−0.004 (2)	0.000
O3	0.0112 (14)	0.0107 (12)	0.0134 (12)	0.000	0.0035 (11)	0.000
O4	0.019 (2)	0.0100 (18)	0.0097 (17)	0.000	0.000	0.000
O5	0.0138 (15)	0.0155 (13)	0.0137 (12)	0.000	−0.0024 (12)	0.000

should lead to appearance of intergrowths/domains of two phases. The holotype shulamitite as an Al-substituted analog of $Ca_3TiFe_2O_8$ is very close to stoichiometric composition in respect to the Ti content. In addition, HRTEM study shows that holotype shulamitite is homogeneous and does not contain any intergrowths with other phases (Fig. 6).

The following main bands are observed in the Raman spectrum of shulamitite (cm^{-1}): 1501 (overtone), 802, 742, 561, 498, 388, 290, 238, 145, 110 (Fig. 7). There are no bands in the OH region. The modes lower than 400 cm^{-1} seem to correspond to the vibrations of the CaO_8 polyhedra and (Fe^{3+},Ti)O_6 octahedra. The modes in the 450–600 and

Table 7. Selected interatomic distances (Å) for shulamitite.

Site			Site		
Ti, Fe1	O4	1.9194 (10)	Ca1	O1	2.273 (3)
	2 × O5	1.9288 (7)		O2	2.336 (3)
	2 × O3	1.9896 (5)		2 × O5	2.3979 (16)
	O1	2.148 (2)		2 × O3	2.5626 (19)
				2 × O1	2.7668 (7)
Al, Fe2	2 × O1	1.759 (3)	Ca2	O4	2.429 (4)
	O2	1.838 (6)		4 × O3	2.5189 (18)
	O2	1.860 (6)		2 × O4	2.7596 (8)
				4 × O5	3.003 (2)

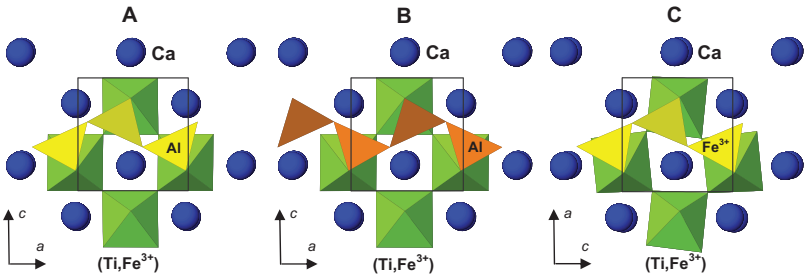

Fig. 4. Crystal structure of shulamitite in space group *Pmma* (A–B) in comparison with synthetic $Ca_3TiFe_2O_8$ (C), space group $Pcm2_1$ (Rodrígues-Carvajal *et al*., 1989). Unit-cell outlines are presented by solid lines. In A–B the two different arrangements of Al-dominant tetrahedra in shulamitite are shown.

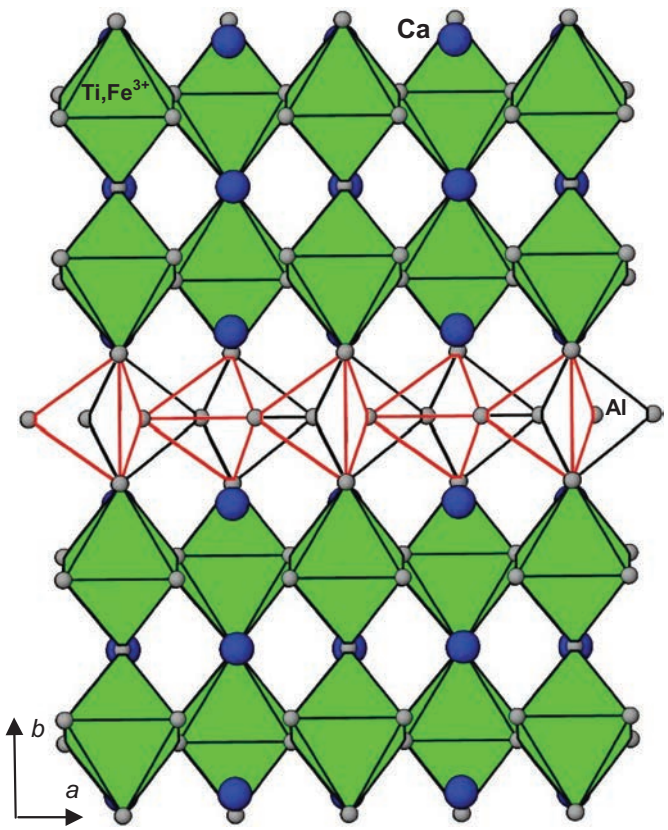

Fig. 5. (001) view of the crystal structures of shulamitite showing the overlay of two orientations of chains of Al-dominant tetrahedra extending along the ***a*** axis.

700–900 cm^{-1} range are related to the bending and stretching vibrations of the $(Al,Fe^{3+})O_4$ tetrahedra.

8. Origin of shulamitite at the Hatrurim Basin

The larnite rocks in the Hatrurim Basin are strongly variable in mineral composition (Gross, 1977, 1984; Sharygin *et al*., 2008). In general, these larnite rocks are the products of the highest-temperature (900–1200 °C) solid-state reactions during combustion metamorphism (Kolodny, 1979; Matthews & Gross, 1980; Sharygin *et al*., 2008) corresponding to the H*T*-region of the spurrite-merwinite facies. However, the absence of reliable indicator minerals or assemblages does not give a possibility to provide a finer subdivision of this temperature interval. According to the $CaTiO_3$–$Ca_2Fe_2O_5$ phase diagram (Becerro *et al*., 1999, 2000, 2002), the minimum formation temperature for some Hatrurim Basin rocks was estimated from the Fe-perovskite–shulamitite paragenesis as 1170–1200 °C (Sharygin *et al*., 2008). Nevertheless, the upper temperature limit for the Hatrurim rocks containing shulamitite and its Fe-analog is not yet known. This may roughly be estimated as 1200–1210 °C based on experimental data (Scarlett *et al*., 2004). In Ca-rich systems with SiO_2 various Ca-bearing ferrites and aluminoferrites (brownmillerite, $CaFe_2O_4$, etc.) are stable up to 1200–1210°C, and with increasing temperature they will react with SiO_2 or Ca-silicates to form Ca-silicoferrites or Ca-aluminosilicoferrites of the aenigmatite-rhönite-dorrite group (Scarlett *et al*., 2004).

Table 8. X-ray diffraction powder data of shulamitite (nine strongest lines are bolded).

Measured		Calculated					Measured		Calculated				
d (Å)	*I*	*d* (Å)	*I*	*h*	*k*	*l*	*d* (Å)	*I*	*d* (Å)	*I*	*h*	*k*	*l*
11.12	***19***	**11.07**	***14***	**0**	**1**	**0**	**1.842**	***16***	**1.845**	***28***	**0**	**6**	**0**
5.55	*11*	5.54	*9*	0	2	0			1.837	*6*	2	2	2
4.99	*5*	4.99	*2*	0	1	1			1.765	*4*	0	2	3
		3.93	*3*	0	2	1	1.758	*2*	1.761	*1*	1	0	3
3.89	***13***	**3.89**	***3***	**1**	**0**	**1**			1.735	*1*	0	5	2
3.697	*5*	3.690	*1*	0	3	0			1.722	*1*	2	3	2
3.190	*2*	3.185	*1*	1	2	1	1.717	*2*	1.716	*1*	2	5	0
3.071	*7*	3.079	*7*	0	3	1	1.658	*5*	1.662	*7*	0	3	3
2.853	*3*	2.793	*30*	0	0	2			1.640	*1*	2	5	1
		2.768	*1*	0	4	0	**1.585**	***17***	**1.589**	***28***	**1**	**3**	**3**
2.755	***40***	**2.750**	***43***	**2**	**0**	**0**	**1.559**	***16***	**1.561**	***22***	**3**	**3**	**1**
2.677	***100***	**2.678**	***100***	**1**	**3**	**1**			1.539	*10*	0	6	2
		2.637	*1*	2	1	0			1.535	*1*	2	0	3
		2.493	*1*	0	2	2	**1.527**	***13***	**1.526**	***13***	**2**	**6**	**0**
		2.483	*3*	1	0	2			1.522	*2*	0	7	1
2.475	*10*	2.480	*12*	0	4	1			1.519	*1*	3	0	2
		2.438	*1*	2	2	0			1.486	*2*	1	4	3
2.420	*2*	2.423	*3*	1	1	2	1.476	*4*	1.481	*2*	1	6	2
		2.385	*1*	2	1	1			1.480	*1*	2	2	3
2.253	*8*	2.256	*11*	1	4	1	1.464	*4*	1.465	*4*	1	7	1
		2.234	*5*	2	2	1			1.462	*2*	3	4	1
2.224	*8*	2.227	*29*	0	3	2			1.462	*1*	2	5	2
2.192	*7*	2.187	*33*	2	3	0	1.412	*3*	1.418	*5*	2	3	3
		2.060	*1*	1	3	2			1.396	*5*	0	0	4
		2.058	*1*	0	5	1	1.385	*4*	1.385	*2*	0	1	4
2.034	*3*	2.037	*4*	2	3	1			1.378	*1*	1	5	3
		1.966	*1*	0	4	2	1.375	*4*	1.376	*1*	0	7	2
1.940	***40***	**1.947**	***73***	**2**	**0**	**2**			1.367	*1*	2	7	0
		1.938	*1*	2	4	0			1.359	*2*	3	5	1
		1.925	*10*	1	5	1	1.357	*6*	1.358	*10*	4	0	0
		1.917	*4*	2	1	2							
		1.848	*3*	1	4	2							

Calculated intensities and *d*-spacings were obtained using CCDC Mercury 2.4 software based on fractional atomic coordinates of shulamitite and cell parameters refined from its powder data: $a = 5.431$ (3), $b = 11.07$ (1), $c = 5.585$ (7) Å.

However, these specific phases are not found in larnite rocks of the Hatrurim Basin.

Dorrite and ''malakhovite'' (Si-poor members of the aenigmatite-rhönite-dorrite group, Grew *et al*., 2008) have been observed in the contact reaction zone between metacarbonate rock and basic paralava from the burned dumps of coal mines in the Chelyabinsk coal basin (Chesnokov *et al*., 1993; Chesnokov, 1997). A dorrite-like phase was also identified in a melilite-larnite rock from the Nabi Musa combustion complex, Hatrurim Formation (Sokol *et al*., 2011). Barioferrite $BaFe_{12}O_{19}$, $CaFe_4O_7$ (''grandiferrite'') and Si-rich srebrodolskite-brownmillerite and Fe-perovskite were found in natural Si-undersaturated buchites (paralavas) from Želénky, Czech Republic (Žáček *et al.*, 2005).

9. Other occurrences of shulamitite and its Fe-analog

Since shulamitite and its Fe-analog have been found at the Hatrurim Basin, Israel (Sharygin *et al*., 2008) and the Upper Chegem volcanic structure, Kabardino-Balkaria, Russia (Galuskin *et al*., 2008, 2011), these phases were also described in other metacarbonate rocks around the world. These occurrences are natural (metacarbonate xenoliths in alkali basalts) or technogenic (metacarbonate fragments in burned dumps of coal mines) in origin (Niedermayr *et al*., 2011; Sharygin, 2011, 2012; Sharygin & Wirth, 2012).

Such metacarbonate rocks are commonly zoned in mineral composition and shulamitite and its Fe-analog are mainly confined to zones near the contact with alkali basalt or pelitic clinker/basic paralava (Sharygin *et al*., 1999; Niedermayr *et al*., 2011; Sharygin, 2011, 2012; Sharygin & Wirth, 2012). These phases are associated with perovskite, brownmillerite and/or srebrodolskite. However, there are no any direct contacts between brownmillerite-srebrodolskite and perovskite (Sharygin *et al*., 2008; Sharygin, 2011, 2012; Sharygin & Wirth, 2012), and there is no contradiction with phase relations in the pseudobinary series $CaTiO_3$–$Ca_2Fe_2O_5$ (Prasanna & Navrotsky, 1994; Becerro *et al*., 1999, 2000, 2002; Cherepanova & Tsybulya, 2008). Figure 8 shows the

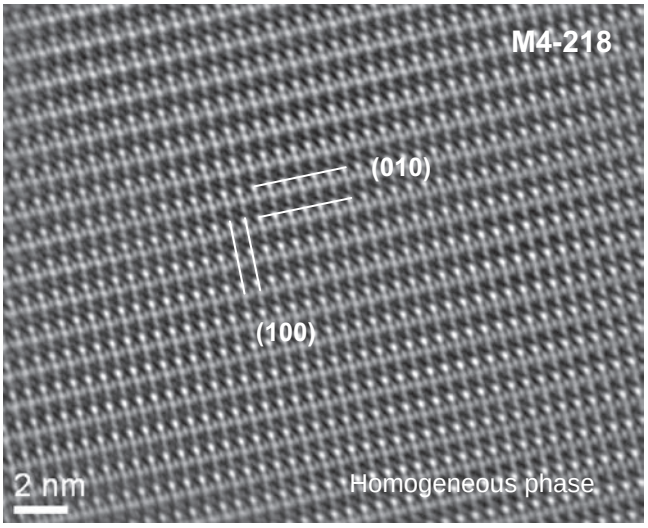

Fig. 6. HRTEM image for holotype shulamitite, Hatrurim Basin.

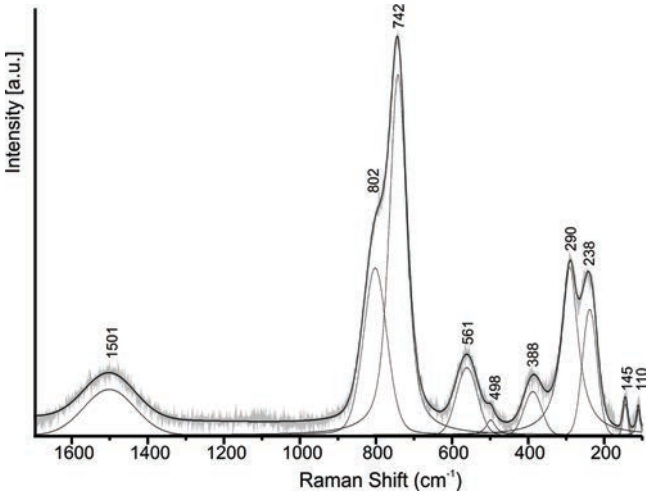

Fig. 7. Raman spectrum of shulamitite (holotype sample).

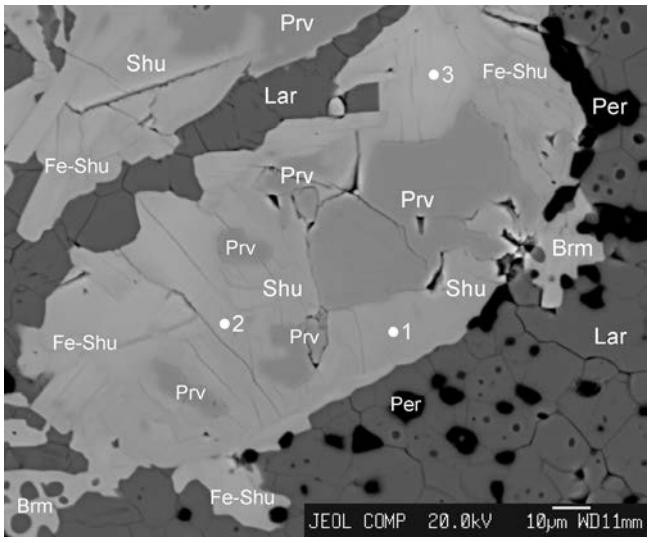

Fig. 8. Shulamitite and its Fe-analog replacing perovskite in a metacarbonate xenolith from alkali basalt (sample E-2011), Bellerberg, E.Eifel, Germany. Prv – perovskite, Fe-Shu – Fe-analog of shulamitite; Per – periclase. Other symbols see in Fig. 1. Points 1–3 see in Table 9.

complex relationships of these phases with perovskite and brownmillerite in a metacarbonate xenolith from alkali basalt, Bellerberg volcano, E. Eifel, Germany. Representative compositions of shulamitite and its Fe-analog from these localities are given in Table 9 and all compositional data are shown in Fig. 9.

In general, broad variations in the content of Fe^{3+} and Al strongly suggest the existence of the $Ca_3TiFeAlO_8$ –$Ca_3TiFeFeO_8$ solid solution. The holotype mineral is close to $Ca_3TiFe(Al_{0.7}Fe_{0.3})O_8$, whereas other compositions from the Hatrurim Basin and other localities show broader variations. The majority of compositions contains SiO_2 (up to 1–2 wt%), ZrO_2 (up 1 wt%), MgO (up to 0.3 wt%), SrO (up to 2 wt%), sometimes Cr_2O_3 (up to 4.5 wt%), MnO and $LREE_2O_3$ (up to 0.5 wt%) (Sharygin *et al*., 2008; Sharygin, 2011, 2012; Sharygin & Wirth, 2012). The ''50% rule'' was used to subdivide shulamitite and Fe-analog in Fig. 9. However, by analogy with the brownmillerite solid solution (Fukuda & Ando, 2002; Redhammer *et al*., 2004; Krüger *et al*., 2009, 2011) the possible existence of two polymorphs and phase transition in the field of Fe-rich compositions should be considered. Unfortunately, there are no experimental data for the system $Ca_3TiAl_2O_8$–$Ca_3TiFe_2O_8$, and the existence of two polymorphs of $Ca_3TiFe(Fe,Al)O_8$ is only assumed due to the similarity in the crystal structures of brownmillerite and shulamitite (presence of octahedral and tetrahedral layers). Compositions richest in Al ($Ca_3TiFeAlO_8 > 90$ mole %, Table 9) are found in metacarbonate rock of the Chelyabinsk coal basin, S. Urals, Russia, whereas Fe-richest species ($Ca_3TiFeFeO_8 > 80$ mole %) occur in metacarbonate xenoliths of E. Eifel, Germany, and Chegem, N. Caucasus, Russia (Fig. 9). Compositions with Al > 1 apfu have not been reported.

Some compositions of shulamitite and its Fe-analog vary in the Ti content (>1.1 and < 0.9 apfu, Fig. 9). According to the phase diagram $CaTiO_3$–$Ca_2Fe_2O_5$ (Becerro *et al*., 1999, 2000, 2002), any deviations from Ti = 1 (apfu) should lead to intergrowths/domains of either $Ca_3TiFe_2O_8$ + $Ca_4Ti_2Fe_2O_{11}$ or $Ca_3TiFe_2O_8$ + brownmillerite. This may be possible in natural and technogenic phases like in cement clinkers (Gloter *et al*., 2000), but all studied shulamitite and its Fe-analog did not show the presence of two micrometer-sized phases. Thus, the Ti deviation may be related to a limited isomorphic substitution in the octahedral sites $2Fe^{3+} \leftrightarrow Ti^{4+}+(Mg,Fe)^{2+}$ or more complex isomorphism involving both octahedral and tetrahedral sites: $^{IV}(Fe,Al)^{3+}+3\ ^{VI}Fe^{3+} \leftrightarrow {}^{IV}Si^{4+}+{}^{VI}Ti^{4+}+2\,{}^{VI}(Mg,Fe)^{2+}$.

Table 9. Chemical composition of shulamitite and its Fe-analog from E.Eifel and other localities.

Sample	1 E-2011	2 E-2011	3 E-2011	4 M7-184	5 M7-184	6 E-2-1	7 E-2-1	8 K-2009	9 42-17g	10 42-17g	11 M-4	12 M-4
n	1	1	1	2	19	1	1	7	12	2	1	4
(wt%)												
SiO_2	0.29	0.32	0.48	0.48	0.71	0.57	0.71	0.61	0.50	0.62	0.67	0.37
TiO_2	20.40	20.63	20.23	21.37	20.98	20.73	18.81	20.30	20.83	19.66	18.67	20.23
ZrO_2	0.09	0.04	0.06	0.17	0.03	n.d.	0.12	0.07	0.48	0.45	0.31	0.41
Nb_2O_5	0.16	0.16	0.17	0.26	0.18	0.19	0.17	0.09	0.06	0.06	0.04	0.06
Cr_2O_3	0.17	0.15	0.13	n.d.	n.d.	0.12	n.d.	n.d.	0.20	0.03	0.02	0.06
V_2O_3					0.13			0.05	n.d.	n.d.	0.18	0.10
Al_2O_3	8.48	6.41	3.43	6.95	3.21	6.42	3.65	5.41	11.79	5.51	4.30	3.55
Fe_2O_3	26.36	28.29	32.12	26.37	30.74	27.39	34.34	30.31	20.32	30.35	33.52	31.95
FeO	0.01	0.04	0.03	0.14	0.51	0.03	0.03		0.11	0.01		0.48
MnO	0.20	0.22	0.22	0.92	0.38	0.18	0.22	0.12	n.d.	n.d.	n.d.	n.d.
MgO	0.06	0.17	0.17	0.71	0.30	n.d.	n.d.	0.21	0.33	0.07	n.d.	n.d.
ZnO	0.04	n.d.	0.03			n.d.	n.d.					
CaO	42.82	42.55	41.89	42.35	41.64	43.04	41.68	42.86	43.68	42.73	41.21	41.10
SrO	0.39	0.52	0.59	0.27	0.55	0.49	0.41	0.37	0.12	0.16	1.41	1.29
La_2O_3								n.d.	0.20	0.13		
Ce_2O_3								n.d.	0.18	0.17		
Na_2O	0.03	n.d.	0.02			0.02	n.d.					
Total	99.50	99.50	99.57	99.99	99.36	99.18	100.14	100.40	98.80	99.95	100.33	99.60
Formulae calculated on 6 cations and 8 oxygens												
Si	0.019	0.021	0.032	0.031	0.047	0.037	0.047	0.004	0.032	0.041	0.044	0.025
Al	0.650	0.497	0.270	0.533	0.253	0.498	0.286	0.417	0.893	0.427	0.337	0.281
Fe^{3+}	0.331	0.482	0.698	0.436	0.700	0.465	0.667	0.543	0.075	0.532	0.619	0.694
Tetrahedra	1.000	1.000	1.000	1.000	1.000	1.000	1.000	1.000	1.000	1.000	1.000	1.000
Ti	0.998	1.019	1.015	1.043	1.055	1.025	0.940	0.997	1.005	0.973	0.932	1.021
Zr	0.003	0.001	0.002	0.005	0.001		0.004	0.002	0.015	0.014	0.010	0.013
Nb	0.005	0.005	0.005	0.008	0.005	0.006	0.005	0.003	0.002	0.002	0.001	0.002
V					0.007			0.003			0.010	0.005
Cr	0.008	0.008	0.007			0.006			0.002	0.002	0.001	0.003
Fe^{3+}	0.960	0.917	0.915	0.854	0.846	0.892	1.051	0.948	0.906	0.971	1.056	0.919
Fe^{2+}	0.001	0.002	0.002	0.008	0.029	0.002	0.001		0.006	0.001		0.027
Mn	0.011	0.012	0.012	0.051	0.021	0.010	0.013	0.007				
Mg	0.006	0.017	0.017	0.069	0.030			0.021	0.032	0.007		
Zn	0.002		0.002									
Octahedra	1.994	1.981	1.977	2.038	1.994	1.941	2.014	1.981	1.978	1.970	2.010	1.990
Ca	2.988	2.999	2.998	2.952	2.985	3.038	2.970	3.005	3.008	3.017	2.936	2.959
Sr	0.015	0.020	0.023	0.010	0.021	0.019	0.016	0.014	0.005	0.006	0.054	0.050
La + Ce									0.009	0.007		
Na	0.003		0.002			0.002						
Polyhedra	3.006	3.019	3.023	2.962	3.006	3.059	2.986	3.019	3.022	3.030	2.990	3.009
End-members												
$Ca_3TiFeAlO_8$	65.03	49.66	26.98	53.24	25.27	49.78	28.59	41.72	89.29	42.72	33.66	28.08
$Ca_3TiFeFeO_8$	33.06	48.22	69.84	43.63	69.99	46.48	66.67	54.29	7.53	53.23	61.90	69.43
$Ca_3Ti(Fe,Mg)SiO_8$	1.91	2.12	3.18	3.13	4.74	3.74	4.74	3.99	3.18	4.05	4.44	2.49

Notes: *n* – number of analyses; Y_2O_3, NiO and K_2O were not determined. Fe_2O_3 and FeO are calculated from charge balance. All alumina is considered to be in the tetrahedral site. 1–7 – metacarbonate xenoliths in alkali basalt, Bellerberg, E.Eifel, Germany: 1–3 – shulamitite and Fe-analog in association with perovskite (author's data, see points 1–3 in Fig. 8); 4–5 – shulamitite and Fe-analog in association with brownmillerite (Sharygin, 2011; author's data); 6 – shulamitite in association with perovskite; 7 – Fe-analog of shulamitite in association with perovskite and brownmillerite; 8 – Fe-analog of shulamitite in association with brownmillerite from a metacarbonate xenolith in olivine nephelinite, Klöc0h, Styria, Austria (author's data); 9–10 – shulamitite and its Fe-analog in association with perovskite from a metacarbonate rock in the contact with parabasalt, burned dump of mine 42, Kopeisk, Chelyabinsk coal basin, Russia (Sharygin, 2012); 11–12 – Fe-analog of shulamitite in association with brownmillerite (11) and perovskite (12) from a metacarbonate rock, burned dump of the Kalinin mine, Donetsk, Donets coal basin, Ukraine (Sharygin, 2011).

10. Concluding remarks

The broad compositional variations for shulamitite and its Fe-analog strongly suggest the existence of the isomorphic series $Ca_3TiFeAlO_8$–$Ca_3TiFeFeO_8$. The appearance of minerals of this series in metacarbonate rocks around the world possibly will be an indicator of high temperature ($\leq$1200 °C) of their formation. The association shulamitite (or Fe-analog) + Fe-perovskite may be used for temperature estimation of high-*T* metacarbonate rocks. The

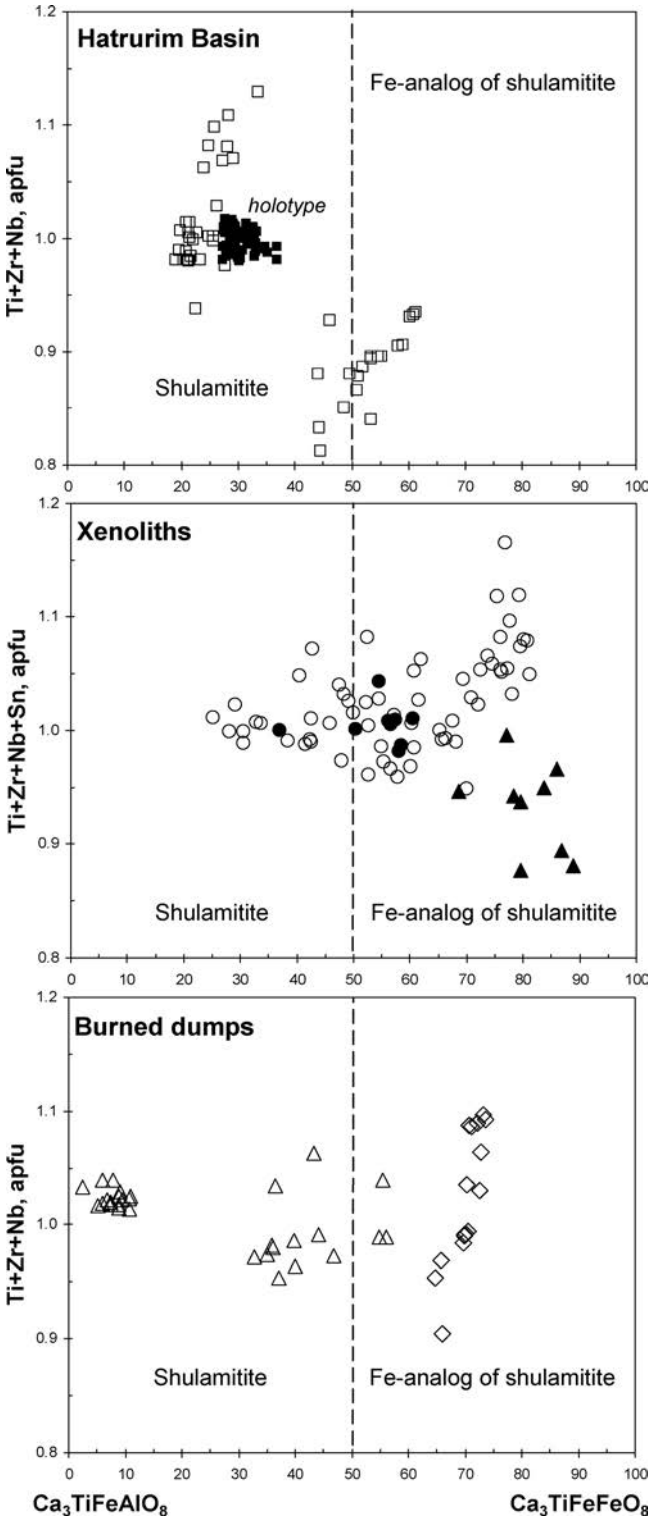

Fig. 9. Compositional variations of shulamitite and its Fe-analog from the Hatrurim Basin, Israel and other localities. Solid squares – holotype shulamitite (sample M4-218); open squares – shulamitite and its Fe-analog from other Hatrurim larnite rocks; open circles – shulamitite and its Fe-analog from metacarbonate xenoliths in alkali basalts, Bellerberg, E.Eifel, Germany; solid circles – shulamitite and its Fe-analog from a metacarbonate xenolith in alkali basalt, Klöch, Styria, Austria; solid triangles – Fe-analog of shulamitite from metacarbonate xenoliths in ignimbrites, Upper-Chegem volcanic structure, Kabardino-Balkaria, Russia; open triangles – shulamitite and its Fe-analog from a metacarbonate rock, burned dump of mine 42, Kopeisk, Chelybinsk coal basin, Russia; open rhombus – Fe-analog of shulamitite from a metacarbonate rock, burned dump of the Kalinin mine, Donetsk, Donets coal basin, Ukraine. New author's data and data from Kolitsch & Brandstätter in Niedermayr *et al*. (2011), Sharygin (2011, 2012), Sharygin & Wirth (2012), and Sharygin *et al*. (2008) were used for plots.

presence of these phases is quite possible in the contact zones between trappean basalts and carbonate strata within platforms.

Acknowledgements: The first author thanks L.N. Pospelova, E.N. Nigmatulina and N.S. Karmanov for help in microprobe analysis and scanning microscopy at the IGM, Novosibirsk. M.P.Mazurov (IGM) and A.N. Fomin (IPGG, Novosibirsk) helped with measurement of microhardness and refraction data for shulamitite. We are grateful to B. Ternes, W. Schüller (Germany), W. Trattner, W. Postl (Austria) and I.V. Pekov (Russia) for donating the samples of metacarbonate xenoliths from alkali basalts. The manuscript was improved through comments and suggestions from the handling editor S.V. Krivovichev and two anonymous reviewers. This work was supported by the Russian Foundation for Basic Research (grant 12-05-00057) and the Russian Ministry of Science and Education (grant 2012-1.5-12-000-1006-001).

References

Becerro, A.I., McCammon, C., Langenhorst, F., Seifert, F., Angel, R.J. (1999): Oxygen-vacancy ordering in $CaTiO_3$–$CaFeO_{2.5}$ perovskites: from isolated defects to infinite sheets. *Phase Trans.*, **69**, 133–146.

Becerro, A.I., Carpenter, M.A., Boffa Ballaran, T., Seifert, F. (2000): Hard mode spectroscopy of $CaTiO_3$–$CaFeO_{2.5}$ perovskites. *Phase Trans.*, **71**, 161–172.

Becerro, A.I., Redfern, S.A.T., Carpenter, M.A., Knight, K.S., Seifert, F. (2002): Displacive phase transitions in and strain analysis of Fe-doped $CaTiO_3$ perovskites at high temperatures by neutron diffraction. *J. Solid State Chem.*, **167**, 459–471.

Bentor, Y.K. & Vroman, A. (1960): The geological map of Israel 1:100000, Sheet 16 – Mount Sedom (with explanatory text). *Geol. Surv. Isr.*, Jerusalem.

Bentor, Y.K., Gross, S., Heller, L. (1963): High temperature minerals in non-metamorphosed sediments in Israel. *Nature*, **199**, 478–479.

Bruker. (2011): SMART and SAINT-Plus (version 6.01). Bruker AXS Inc., Madison, WI.

Burg, A., Starinsky, A., Bartov, Y., Kolodny, Ye. (1991): Geology of the Hatrurim Formation (''Mottled Zone'') in the Hatrurim basin. *Isr. J. Earth Sci.*, **40**, 107–124.

Burg, A., Kolodny, Ye., Lyakhovsky, V. (1999): Hatrurim-2000: the ''Mottled Zone'' revisited, forty years later. *Isr. J. Earth Sci.*, **48**, 209–223.

Cherepanova, S.V. & Tsybulya, S.V. (2008): Peculiarities of the X-ray diffraction of oxygen-deficient perovskite-related materials with partial vacancy ordering. *Z. Kristallogr.*, **27**, Suppl., 5–12.

Chesnokov, B.V. (1997): Silicooxides in products of burning in dumps of coal pits. *Dokl. Akad. Nauk.*, **356**, 3, 374–375.

Chesnokov, B.V., Vilisov, V.A., Bazhenova, L.F., Bushmakin, A.F., Kotlyarov, V.A. (1993): New minerals from burned spoil-heaps of the Chelyabinsk coal basin (fifth report). *Ural. Mineral. Sbornik.*, **2**, 3–36 (in Russian).

Fukuda, K. & Ando, H. (2002): Determination of the *Pcmn*/*Ibm*2 phase boundary at high temperature in the system $Ca_2Fe_2O_5$–$Ca_2Al_2O_5$. *J. Am. Ceram. Soc.*, **85**, 1300–1303.

Galuskin, E.V., Gazeev, V.M., Armbruster, T., Zadov, A.E., Galuskina, I.O., Pertsev, N.N., Dzierżanowski, P., Kadiyski, M., Gurbanov, A.G., Wrzalik, R., Winiarski, A. (2008): Lakargiite $CaZrO_3$: a new mineral of the perovskite group from the North Caucasus, Kabardino-Balkaria, Russia. *Am. Mineral.*, **93**, 1903–1910.

Galuskin, E.V., Galuskina, I.O., Gazeev, V.M., Dzierżanowski, P., Prusik, K., Pertsev, N.N., Zadov, A.E., Bailau, R., Gurbanov, A.G. (2011): Megawite, $CaSnO_3$: a new perovskite-group mineral from skarns of the Upper Chegem caldera, Kabardino-Balkaria, Northern Caucasus, Russia. *Mineral. Mag.*, **75**, 2563–2572.

Galuskin, E.V., Grew, E.S., Galuskina, I.O., Armbruster, T., Bailau, R. (2012): The mayenite supergroup: A reexamination of mayenite and related minerals. *in* ''Abstracts of the European Mineralogical Conference''. Goethe University, Frankfurt on Main, **Vol. 1**, EMC2012-54-2, CD-Edition.

Gloter, A., Ingrin, J., Bouchet, D., Scrivener, K., Colliex, C. (2000): TEM evidence of perovskite-brownmillerite coexistence in the $Ca(Al_xFe_{1-x})O_{2.5}$ system with minor amounts of titanium and silicon. *Phys. Chem. Minerals.*, **27**, 504–513.

Gonzáles-Calbet, J.M. & Valett-Regí, M. (1987): A new perovskite-type compound: $Ca_4Fe_2Ti_2O_{11}$. *J. Solid State Chem.*, **68**, 266–272.

Grenier, J.-C., Darriet, J., Pouchard, M., Hagenmuller, P. (1976): Mise en evidence d'une nouvelle famille de phases de type perovskite lacunaire ordonnée de formule $A_3M_3O_8$ ($AMO_{2.67}$). *Mat. Res. Bull.*, **11**, 1219–1226.

Grenier, J.-C., Schiffmacher, G., Caro, P., Pouchard, M., Hagenmuller, P. (1977): Etude par diffraction X et microscopie électronique du système $CaTiO_3$–$CaFe_2O_5$. *J. Solid State Chem.*, **20**, 365–379.

Grew, E.S., Hålenius, U., Pasero, M., Barbier, J. (2008): Recommended nomenclature for the sapphirine and surinamite groups (sapphirine supergroup). *Mineral. Mag.*, **72**, 839–876.

Gross, S. (1977): The mineralogy of the Hatrurim Formation, Israel. *Geol. Surv. Isr. Bull.*, **70**, 80 p.

— (1980): Bentorite, a new mineral from the Hatrurim area, West of the Dead Sea, Israel. *Isr. J. Earth Sci.*, **29**, 81–84.

— (1984): Occurrence of ye'elimite and ellestadite in an unusual cobble from the ''pseudo-conglomerate'' of the Hatrurim Basin, Israel. *Geol. Surv. Isr.*, *Current Research 1983–84*, 1–4.

Gross, S. & Heller, L. (1963): A natural occurrence of bayerite. *Mineral. Mag.*, **33**, 723–724.

Gur, D., Steinitz, G., Kolodny, Y., Starinsky, A., McWilliams, M. (1995): $^{40}Ar/^{39}Ar$ dating of combustion metamorphism (''Mottled Zone'', Israel). *Chem. Geol.*, **122**, 171–184.

Hatert, F. & Burke, E.A.J. (2008): The IMA-CNMNC dominant-constituent rule revisited and extended. *Can. Mineral.*, **46**, 717–728.

Kolodny, Y. (1979): Natural cement factory: a geological story. *in* ''Cement Production and Use'', J. Skalny, ed. Franklin Pierce College, Rindge, New Hampshire, 203–216.

Krüger, H., Kahlenberg, V., Petricek, V., Phillipp, F., Wertl, W. (2009): High-temperature structural phase transition in $Ca_2Fe_2O_5$ studied by in-situ X-ray diffraction and transmission electron microscopy. *J. Solid State Chem.*, **182**, 1515–1523.

Krüger, H., Stöber, S., Welberry, T.R., Withers, R.L., Gerald, J.D.F. (2011): Stacking faults and superstructures in a layered brownmillerite. *Acta Crystallogr.*, **B67**, 476–485.

Marinho, M.B. & Glasser, F.P. (1984): Polymorphism and phase changes in the ferrite phase of cements induced by titanium substitution. *Cement Concrete Res.*, **14**, 360–368.

Matthews, A. & Gross, Sh. (1980): Petrologic evolution of the ''Mottled Zone'' (Hatrurim) metamorphic complex of Israel. *Isr. J. Earth Sci.*, **29**, 93–106.

Murashko, M.N., Chukanov, N.V., Mukhanova, A.A., Vapnik, Ye., Britvin, S.N., Krivovichev, S.V., Polekhovsky, Y.S., Ivakin, I.D. (2011): Barioferrite $BaFe^{3+}{}_{12}O_{19}$: a new mineral species of the magnetoplumbite group from the Hatrurim Formation in Israel. *Geol. Ore Deposits*, **53**, 7, 558–563.

Niedermayr, G., Auer, C., Bernhard, F., Brandstätter, F., Gröbner, J., Hammer, V.M.F., Knobloch, G., Koch, G., Kolitsch, U., Konzett, J., Leikauf, B., Löffler, E., Postl, W., Prasnik, H., Prayer, A., Pristacz, H., Sabor, M., Seemann, R., Stehlik, H., Thinschmidt, A., Walter, F. (2011): Neue Mineralfunde aus Österreich LX. *Carinthia II*, **201./121**., 135–186.

Prasanna, T.S.R. & Navrotsky, A. (1994): Energetics in the brownmillerite-perovskite pseudobinary $Ca_2Fe_2O_5$–$CaTiO_3$. *J. Mat. Res.*, **9**, 12, 3121–3124.

Redhammer, G.J., Tippelt, G., Roth, G., Amthauer, G. (2004): Structural variations in the brownmillerite series $Ca_2(Fe_{2-x}Al_x)O_5$: single-crystal X-ray diffraction at 25 °C and high-temperature powder diffraction ($25°C \leq T \leq 1000$ °C). *Am. Mineral.*, **89**, 405–420.

Rodrígues-Carvajal, J., Valett-Regí, M., González-Calbet, J.M. (1989): Perovskite threefold superlattices: a structure determination of the $A_3M_3O_8$ phase. *Mat. Res. Bull.*, **24**, 423–430.

Scarlett, N.V.Y., Pownceby, M.I., Madsen, I.C., Christensen, A.N. (2004): Reaction sequences in the formation of silico-ferrites of calcium and aluminum in iron ore sinter. *Metall. Mater. Trans. B*., **35B**, 929–936.

Sharygin, V.V. (2011): Lakargiite and minerals of the perovskite-brownmillerite series in metacarbonate rocks from Donetsk burned dumps. *Proc. Donetsk Nat. Techn. Univer. Min. Geol. Ser.*, **15**, 192, 114–125 (in Russian).

— (2012): Minerals of the $Ca_3TiFeAlO_8$ – $Ca_3TiFeFeO_8$ series in natural and technogenic pyrometamorphic systems. *in* ''The Mineralogy of Technogenesis-2012'', S.S. Potapov, ed. Institute of Mineralogy, Uralian Branch of Russian Academy of Sciences, Miass, 29–49 (in Russian).

Sharygin, V.V. & Wirth, R. (2012): Shulamitite and its Fe-analog in metacarbonate xenoliths from alkali basalts, E. Eifel, Germany. *in* ''Abstracts of 29th international conference ore potential of alkaline, kimberlite and carbonatite magmatism'', School ''Alkaline magmatism of the Earth'', Sudak - Mosow, OUTI GEOKHI RAS, 97–99, http://alkaline. web.ru/2012/abstracts.htm

Sharygin, V.V., Sokol, E.V., Nigmatulina, E.N., Lepezin, G.G., Kalugin, V.M., Frenkel', A.E. (1999): Mineralogy and petrography of technogenic parabasalts from the Chelyabinsk brown-coal basin. *Geol. Geofiz.*, **40**, 6, 896–915.

Sharygin, V.V., Vapnik, Ye., Sokol, E.V., Kamenetsky, V.S., Shagam, R. (2006): Melt inclusions in minerals of schorlomite-rich veins of the Hatrurim Basin, Israel: composition and homogenization temperatures. *in* ''ACROFI I program with abstracts'', P. Ni and Z. Li, eds. Nanjing University PH, China. 189–192.

Sharygin, V.V., Sokol, E.V., Vapnik, Y. (2008): Minerals of the pseudobinary perovskite-brownmillerite series from combustion metamorphic larnite rocks of the Hatrurim Formation (Israel). *Russ. Geol. Geophys.*, **49**, 10, 709–726.

Sheldrick, G.M. (1996): SADABS. University of Göttingen, Germany.

— (2008): A short history of SHELX. *Acta Crystallogr.*, **A64**, 112–122.

Sokol, E.V., Maksimova, N.V., Nigmatulina, E.N., Sharygin, V.V., Kalugin, V.M. (2005): Combustion Metamorphism. Izd. SO RAN, Novosibirsk. 284 p. (in Russian).

Sokol, E.V., Novikov, I.S., Vapnik, Ye., Sharygin, V.V. (2007): Gas fire from mud volcanoes as a trigger for the appearance of high-temperature pyrometamorphic rocks of the Hatrurim Formation (Dead Sea area). *Dokl. Earth Sci*., **413A**, 3, 474–480.

Sokol, E.V., Novikov, I.S., Zateeva, S.N., Sharygin, V.V., Vapnik, Ye. (2008): Pyrometamorphic rocks of the spurrite-merwinite facies as indicators of hydrocarbon discharge zones (the Hatrurim Formation, Israel). *Dokl. Earth Sci.*, **420**, 4, 608–614.

Sokol, E., Novikov, I., Zateeva, S., Vapnik, Ye., Shagam, R., Kozmenko, O. (2010): Combustion metamorphic rocks as indicators of fossil mud volcanism: New implications for the origin of the Mottled Zone, Dead Sea rift area. *Basin Res.*, **22**, 414–438.

Sokol, E.V., Gaskova, O.L., Kokh, S.N., Kozmenko, O.A., Seryotkin, Y.V., Vapnik, Y., Murashko, M. (2011): Chromatite and its Cr^{3+}- and Cr^{6+}-bearing precursor minerals from the Nabi Musa Mottled Zone complex, Judean Desert. *Am. Mineral.*, **96**, 659–674.

Sokol, E.V., Kozmenko, O.A., Kokh, S.N., Vapnik, Y. (2012): Gas reservoirs in the Dead Sea area: evidence from chemistry of combustion metamorphic rocks in the Nabi Musa fossil mud volcano. *Russ. Geol. Geophys.*, **53**, 8, 745–762.

Vapnik, Y., Sokol, E., Murashko, M., Sharygin, V. (2006): The enigma of Hatrurim. *Mineral. Almanac*., **10**, 69–77.

Vapnik, Y., Sharygin, V.V., Sokol, E.V., Shagam, R. (2007): Paralavas in combustion metamorphic complex at the Hatrurim Basin, Israel. *in* ''Geology of Coal Fires: Case Studies from Around the World'', G. Stracher, ed., *GSA Rev. Eng. Geol*., **XVIII**, 133–153.

Weber, D. & Bischoff, A. (1994): Grossite ($CaAl_4O_7$) – a rare phase in terrestrial rocks and meteorites. *Eur. J. Mineral.*, **6**, 591–594.

Wirth, R. (2009): Focused Ion Beam (FIB) combined with SEM and TEM: advanced analytical tools for studies of chemical composition, microstructure and crystal structure in geomaterials on a nanometer scale. *Chem. Geol.*, **261**, 217–229.

Žáček, V., Skála, R., Chlupáčová, M., Dvorák, Z. (2005): Ca–Fe^{3+}-rich Si-undersaturated buchite from Želénky, North-Bohemian brown coal basin, Czech Republic. *Eur. J. Mineral.*, **17**, 623–633.

Zateeva, S.N., Sokol, E.V., Sharygin, V.V. (2007): Specificity of pyrometamorphic minerals of the ellestadite group. *Geol. Ore Deposits*, **49**, 8, 792–805.

Received 31 July 2012
Modified version received 31 August 2012
Accepted 11 September 2012